



Effect of the external electric fields on the polarization and vibrational spectrum of 1-ethyl-3-methylimidazolium bis(trifluoromethylsulfonyl)imide on graphene surface

Yongji Guan^a, Chuyu Li^a, Xin Han^a, Huanwang Jing^c, Fulong Yang^d, Xiaoping Zhang^{a,*}, Youquan Deng^{b,*}

^a Institute of Optoelectronics and Electromagnetic Information, School of Information Science and Engineering, Lanzhou University, Lanzhou 730000, People's Republic of China

^b Centre for Green Chemistry and Catalysis, Lanzhou Institute of Chemical Physics, Chinese Academy of Sciences, Lanzhou 730000, People's Republic of China

^c State Key Laboratory of Applied Organic Chemistry, College of Chemistry and Chemical Engineering, Lanzhou University, Lanzhou 730000, People's Republic of China

^d College of Electrical and Information Engineering, Lanzhou University of Technology, Lanzhou 730050, People's Republic of China

ARTICLE INFO

Keywords:

Ionic liquid
Graphene surface
Density functional theory
Vibrational spectrum
External electric fields

ABSTRACT

Ionic liquids, emerging as innovative solvents for energy harvesting, necessitate a comprehensive understanding of their structural characteristics at the graphene-ionic liquid interface. This work delves into the effects of external electric fields (EEFs) on the polarization and vibrational spectrum of 1-ethyl-3-methylimidazolium bis(trifluoromethylsulfonyl)imide ([Emim][NTf₂]) on a graphene surface, employing density functional theory calculations. The analysis reveals that the geometrical configuration and stability of functional groups within the graphene-[Emim][NTf₂] system are influenced by both the direction and intensity of the applied EEF. Notably, the threshold EEF strength required for dissociation varies based on the structural configuration of the anion. The electronic energy, dipole moment, and polarization rate under varying EEF conditions have been quantitatively assessed, providing insights into their EEF-dependent behaviors. Utilizing the independent gradient model approach, the inter-ion interactions, such as hydrogen bonding and van der Waals forces, under the influence of EEFs were analyzed, and how these interactions evolve with changes in the direction and intensity of the EEFs were also explored. Furthermore, the vibrational spectrum of [Emim][NTf₂] on the graphene surface, spanning a range of 10–3500 cm⁻¹, was meticulously calculated to systematically investigate the impact of the EEF on the vibrational spectra of the graphene-[Emim][NTf₂] system. A key finding of this work is the distinct shifts in the vibrational peaks of the *cis* and *trans* isomers of [NTf₂]⁻ on the graphene surface, which can be attributed to differences in their exchange energies. Specifically, the exchange energy for the *cis* isomer of [NTf₂]⁻ is measured at 107.43 kJ•mol⁻¹, in contrast to 98.51 kJ•mol⁻¹ for the *trans* isomer.

1. Introduction

Ionic Liquids (ILs) are a distinct class of ionic compounds, characterized by their composition of anions and cations, which predominantly exist as liquids at or near ambient temperature [1–3]. Recognized for their environmentally-friendly nature, these solvents exhibit a comprehensive array of advantageous physicochemical properties, including but not limited to low vapor pressure, minimal volatility, high thermal and chemical stability, facile purification and separation processes, robust electrical conductivity, and an expansive electrochemical window [4–7]. Such properties have propelled their utilization in diverse

domains, including separation [8,9], catalysis [4,5,7,10–15], electrochemistry [16–19], energy harvesting [20–24], (electro-)wetting [25,26], variable focus lenses [27], lab-on-a-chip systems [28], among others [29]. Given their widespread utility, understanding the structural and dynamic intricacies of ILs becomes paramount for both academic research and industrial applications. The vibrational spectrum (VS), serves as an invaluable analytical tool for elucidating the structural intricacies of ILs, including the identification of conformational functional groups and hydrogen bonding interactions [30–35].

Extensive research has been conducted on the VS of ILs, employing both experimental and computational approaches to elucidate

* Corresponding authors.

E-mail addresses: zxp@lzu.edu.cn (X. Zhang), yqeng@licp.cas.cn (Y. Deng).

<https://doi.org/10.1016/j.molliq.2024.125313>

Received 13 December 2023; Received in revised form 9 May 2024; Accepted 18 June 2024

Available online 19 June 2024

0167-7322/© 2024 Elsevier B.V. All rights reserved, including those for text and data mining, AI training, and similar technologies.

molecular structures and interaction energies between anions and cations. Heimer et al. [36] utilized density functional theory (DFT) to investigate the IR spectra of 1-alkyl-3-methylimidazolium tetrafluoroborate ILs ([C_nmim][BF₄]). Their work revealed hydrogen bonding interactions between the fluorine atoms of the [BF₄][−] anion and the C2 hydrogen on the imidazolium ring. Booth and Vyas et al. [37,38] investigated multiple conformers of 1-ethyl-3-methylimidazolium bis(trifluoromethylsulfonyl)imide ([Emim][NTf₂]) in the gas phase using IR/UV action spectroscopy and found each conformer has a characteristic red shift in the frequency of its C2–H group that reveals the variation in strength of a hydrogen bond between the cation and anion. Roth et al. [39] investigated hydrogen bonding in [Emim][NTf₂] by linear and nonlinear vibrational spectroscopy, and the results support the hypothesis of weak hydrogen bonding involving the C4–H and C5–H groups and somewhat stronger hydrogen bonds of the C2–H groups. Grondin et al. [40] investigated the VS of [Emim][NTf₂] combined IR and Raman spectroscopies with DFT calculations, and found the stretching vibration of the quasi-diatom C2–D bond appears to be a good spectroscopic probe of the increasing cation–anion interactions when the coordinating strength of the anion increases. Fumino et al. [34,41] combined Far IR spectroscopy with DFT calculations to study cation–anion and cation–solvent interactions in solutions of the IL triethylammonium iodine. They found that increasing temperature led to a reformation of the vibrational peaks of contact ion pairs, attributable to reduced solvent polarity. Shirota et al. [31,33] studied the ultrafast dynamics of 40 (non-)aromatic cation based ILs by means of femtosecond Raman induced Kerr effect spectroscopy, and found the aromatic cation based ILs show a different relation of the first moment of the low-frequency spectral band to the bulk liquid parameter and the spectral intensity in nonaromatic cation based ILs was much lower than that in aromatic cation based ILs owing to the absence of the aromatic ring. Velpula et al. [42] employed molecular dynamics (MD) simulations and Raman spectroscopy to analyze [C_nmim][BF₄] ILs on graphene surface. They discovered that these ILs induce n-type doping in graphene, with the extent of doping increasing with cation chain length, contrary to the expected decrease in surface-adsorbed ion density. This phenomenon was attributed to changes in the electrostatic potential at the graphene-IL interface. Zhang et al. [30] applied DFT calculations to systematically investigate the VS of [Emim][BF₄] on a graphene surface across a frequency range of 10 to 3500 cm^{−1}. Their findings indicated that shifts in the VS were primarily due to interactions between graphene and the [BF₄][−] anion, governed by induction (63.43 %) and dispersion (34.37 %) interaction. Guan et al. [43] employed both DFT calculations and MD simulations to explore the dynamic changes in the Terahertz (THz)-frequency IR of 1-butyl-3-methylimidazolium dicyanamide in the 30 to 300 cm^{−1} range on a graphene surface. They concluded that shifts in the THz IR were due to the formation of a stronger adsorbed layer at the graphene-IL interface, which enhanced hydrogen bonding between cations and anions and constrained the torsional and out-of-plane bending motions of the CH₃ group.

While extensive research has been conducted the VS of ILs, there remains a paucity of studies examining the VS of ILs under the influence of external electric fields (EEFs) using DFT. A notable exception is the work by Bardak et al. [44], who employed DFT to investigate the behavior of 1-hexyl-3-methylimidazolium chloride under an applied EEF. Their findings revealed that both the inter-ion bond and molecular conformation of the IL are susceptible to modulation by the strength and orientation of the EEF, with ion dissociation observed at 0.7 V Å^{−1}. Furthermore, time-dependent DFT calculations highlighted that the UV–visible spectra and associated electron leap properties are contingent upon the EEF direction. Notably, an observed redshift in the UV–visible spectra with increasing induction suggests heightened excitation susceptibility of the IL. Welton et al. [45,46] investigated the effect of an EEF on the dynamics and intramolecular structures of ions in [Bmim][NTf₂] by MD simulations, and confirm that the charge arms of ions align with and stretch out along the EEFs. Maginn et al. [47] probed

the influence of EEFs on the glass transition temperature of [Emim][NTf₂] and found the EEF lowers the activation energy for diffusion reducing the energetic barrier for movement and consequently glass transition temperature by examining the dynamics and structure of the liquid phase. In this work, the polarization and VS of [Emim][NTf₂] on a graphene surface in the presence of EEFs are investigated. The rationale for selecting [Emim][NTf₂] was that [NTf₂][−] exhibits interesting behaviors due to diffuse charge distribution and the delocalized negative charge along the S–N–S core. The delocalized negative charge in [NTf₂][−] allows the formation of low melting, high ionic conductivity, fluid IL when paired with the [Emim]⁺, which had been previously selected by our group for energy harvesting and electromagnetic wave absorption studies in the graphene-[Emim][NTf₂] system. Our investigation extends to the modulation of the weak interactions of the system by the EEFs. A key finding of this work was the distinct VS of [Emim][NTf₂] corresponding to varying graphene-[Emim][NTf₂] conformations under EEFs. The findings of this work serve as the foundation for subsequent investigations into the polarization and VS of bulk [Emim][NTf₂] on graphene surface under the influence of the EEFs. Meanwhile, this work provides a clear demonstration of the polarization and VS of [Emim][NTf₂] ion pair on a graphene surface under the EEFs, which is challenging to observe but crucial in bulk [Emim][NTf₂] and graphene system.

2. Theoretical methods

2.1. Electronic structure calculation

In this work, the first objective was to identify the most stable configuration of the [Emim][NTf₂] ion pair. To achieve this goal, the genmer program within the Molclus software suite [48] was utilized to randomly generate 20 initial structures for both the *cis* and *trans* isomers. These initial structures of the [Emim][NTf₂] ion pair were subsequently optimized using Gaussian 16 [49], employing the B3LYP-D3/TZVP level of theory [50,51]. Following this, the most stable *cis* and *trans* isomers were adsorbed onto a graphene surface (Fig. 1) for further optimization and vibrational frequency calculations, also performed at the B3LYP-D3/TZVP level. Within the graphene-[Emim][NTf₂] system, the graphene surface was designated as the reference plane (*xoy*), and the vector extending from the nitrogen atom connected to the ethyl chain to the nitrogen atom connected to the methyl chain was defined as the positive *x* direction. An EEF was applied in increments of 0.001 a.u. in the specified positive *x* and *z* directions until molecular dissociation was observed. It is noteworthy that 1 a.u. is approximately equivalent to 51.423 V Å^{−1}. Importantly, all frequency calculations were devoid of imaginary frequencies, thereby confirming the stability of the optimized structures.

2.2. Weak interactions between graphene and [Emim][NTf₂]

The independent gradient model (IGM) was employed to investigate the weak forces between graphene and [Emim][NTf₂] [52]. The model is mathematically represented by the following equations:

$$g^{\text{inter}}(\mathbf{r}) = \left| \sum_A \sum_{i \in A} \nabla \rho_i(\mathbf{r}) \right| \quad (1)$$

$$g^{\text{GM,inter}}(\mathbf{r}) = \left| \sum_A \text{abs} \left[\sum_{i \in A} \nabla \rho_i(\mathbf{r}) \right] \right| \quad (2)$$

$$\delta[g^{\text{inter}}(\mathbf{r})] = g^{\text{GM,inter}}(\mathbf{r}) - g^{\text{inter}}(\mathbf{r}) \quad (3)$$

$$\delta[g^{\text{inter}}(\mathbf{r})] = \delta[g(\mathbf{r})] - \delta[g^{\text{inter}}(\mathbf{r})] \quad (4)$$

In these equations, *A* denotes the fragment number, *i* signifies the atomic number, and ∇ρ is the gradient vector. Specifically, Eq. (2)

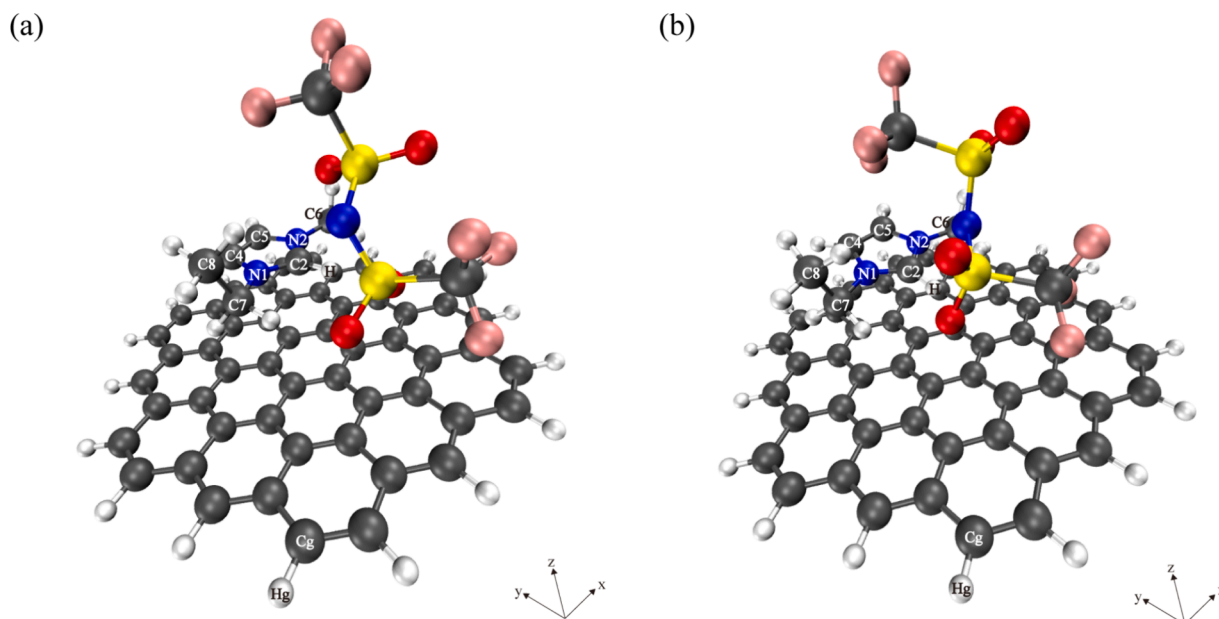


Fig. 1. The initial structure of graphene-[Emim][NTf₂] system, where anion is (a) *cis* isomer and (b) *trans* isomer.

encapsulates the absolute value of each component within the gradient vector $\nabla\rho$. The term represents the modulus of the gradient vector, and δg is indicative of the interactions among all atoms within the system under consideration. The blue/red/green lobes are colored by formula (4) for non-covalent interactions on an RGB scale, with strong mutual repulsion in red, van der Waals interactions in green, and strong attraction interactions such as hydrogen bonding in blue. Specifically, the blue lobes correspond to regions where the formula (2) is positive, the red lobes correspond to regions where the formula (2) is negative, and the green lobes correspond to regions where the absolute value of the formula (3) is large.

2.3. Optical properties

How the dipole moment μ responds to changes within the graphene-[Emim][NTf₂] system was examined in our investigation. The dipole moment, expressed in Debye, is derived from the components associated with each coordinate axis, as represented by:

$$\mu_{\text{total}} = \sqrt{\mu_x^2 + \mu_y^2 + \mu_z^2} \quad (5)$$

Furthermore, the work leveraged the components of the polarizability tensor α_{xx} , α_{yy} and α_{zz} to compute both the mean polarizability α and the anisotropic polarizability $\Delta\alpha$, as detailed in:

$$\alpha = (\alpha_{xx} + \alpha_{yy} + \alpha_{zz})/3 \quad (6)$$

$$\Delta\alpha = \sqrt{[(\alpha_{xx} - \alpha_{yy})^2 + (\alpha_{xx} - \alpha_{zz})^2 + (\alpha_{yy} - \alpha_{zz})^2 + 6(\alpha_{xy}^2 + \alpha_{xz}^2 + \alpha_{yz}^2)]/2} \quad (7)$$

2.4. Molecular polarity index (MPI)

In this section, the assessment of the polarity of the system is investigated, which is determined by the distribution of the electrostatic potential on the molecular surface. The MPI [53] serves as a metric to gauge the polarizable characteristics of the molecule, as described by:

$$\text{MPI} = (1/B) \iint_S |V(\mathbf{r})| dS \quad (8)$$

In this equation, V represents the molecular electrostatic potential, S denotes the molecular surface, and B signifies the molecular surface area. It is noteworthy that a larger MPI value is indicative of a molecule with heightened overall polarity.

3. Results and discussion

3.1. Geometric structure

In this section, the *cis* and *trans* isomers of [NTf₂]⁻ were first optimized. The calculated energy minima for the *trans* and *cis* isomers of [NTf₂]⁻ were found to be 0 kJ mol⁻¹ (-2172.531283 Hartree) and 3.28 kJ mol⁻¹, respectively. Then the ion pairs of the above mentioned most stable structures were selected to bind with graphene facets, respectively, and the geometrical structure of the graphene-[Emim][NTf₂] system was optimized in the absence of an EEF. The computed total energies for graphene-[Emim][NTf₂] with the *cis* and *trans* isomers were 0 kJ mol⁻¹ (-4242.348831 Hartree) and 3.57 kJ mol⁻¹, respectively, with corresponding dipole moments of 8.860563 Debye and 10.554658 Debye. When subjected to an EEF, the optimization of the graphene-[Emim][NTf₂] systems were performed in the z direction, with limiting fields ranging from -0.01 a.u. to 0.005 a.u. for the *cis* structure and from -0.008 a.u. to 0.007 a.u. for the *trans* structure. For calculations in the x direction, EEF values between -0.005 and 0.005 a.u. were selected to mitigate the influence of hydrogen atoms from [Emim][NTf₂] located at the graphene edges. It is noteworthy that when the applied field strength surpassed these limits, chemical bond dissociation was observed, preventing the optimization from converging.

The geometric analysis revealed that the imidazolium ring of [Emim]⁺ is proximal to the graphene surface. To provide a comprehensive visualization of the relative positions between graphene and [Emim][NTf₂], the electrostatic surface potential (ESP) method was employed. This ESP was computed using Multiwfn [54] for both *cis* and *trans* configurations of the graphene-[Emim][NTf₂] system and subsequently visualized using the VMD software [55], as depicted in Fig. 2. In this representation, regions of positive potential are highlighted in red, while negative potential areas are shown in blue. Notably, the [Emim]⁺

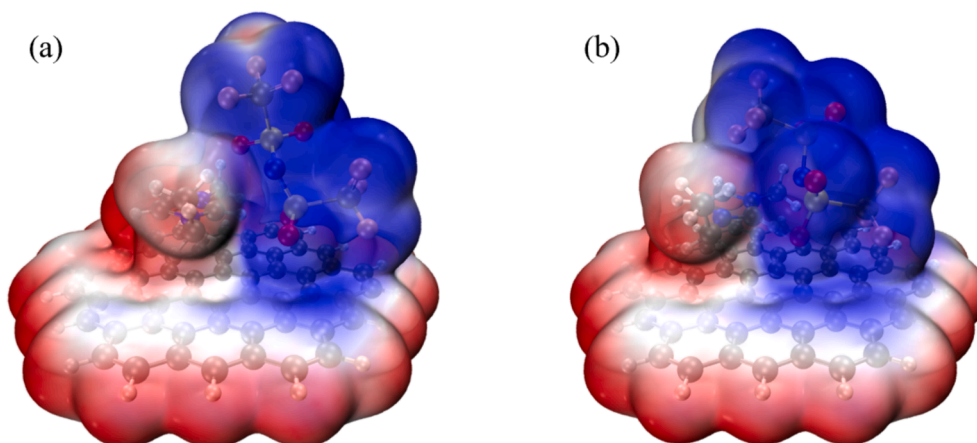


Fig. 2. ESP of graphene-[Emim][NTf₂] system, where the anion is (a) *cis* isomer and (b) *trans* isomer. The red and blue isosurfaces represent the areas with positive and negative electrostatic potentials respectively. (For interpretation of the references to colour in this figure legend, the reader is referred to the web version of this article.)

ion exhibits an attraction towards the graphene, a phenomenon attributed to the complementary positive and negative potentials, enhancing the stability of the system. The cationic component, [Emim]⁺, aligns closely and parallel to the graphene surface. Similarly, the anionic counterpart, [NTf₂]⁻, also demonstrates an affinity towards the graphene, with one of its ends aligning parallel to the graphene plane.

To elucidate the alterations in the relative positioning of graphene and [Emim][NTf₂] under the influence of EEFs, the IGM was employed. This model delineates the varying interactions within the system. Specifically, regions colored blue signify interactions that, despite being weak, exhibit strong attractive behavior, akin to hydrogen bonding. The green regions represent even weaker interactions, characteristic of van der Waals forces. Conversely, the red–orange regions depict mutual atomic repulsions. Fig. 3 provides a visual representation of the weak interactions exhibited by the *cis* isomer of the graphene-[Emim][NTf₂] system under EEFs in the *x* direction. Upon the application of EEFs along this direction, the [NTf₂]⁻ ion is observed to be drawn closer to the graphene surface, leading to a predominant alteration in their mutual interactions. Notably, when the EEF strength surpasses a certain threshold, the C-F bond within [NTf₂]⁻ engages with the edge of the graphene. This interaction culminates in the disruption of the interatomic chemical bonds within the graphene-[Emim][NTf₂] system, thereby inhibiting the formation of a stable structure.

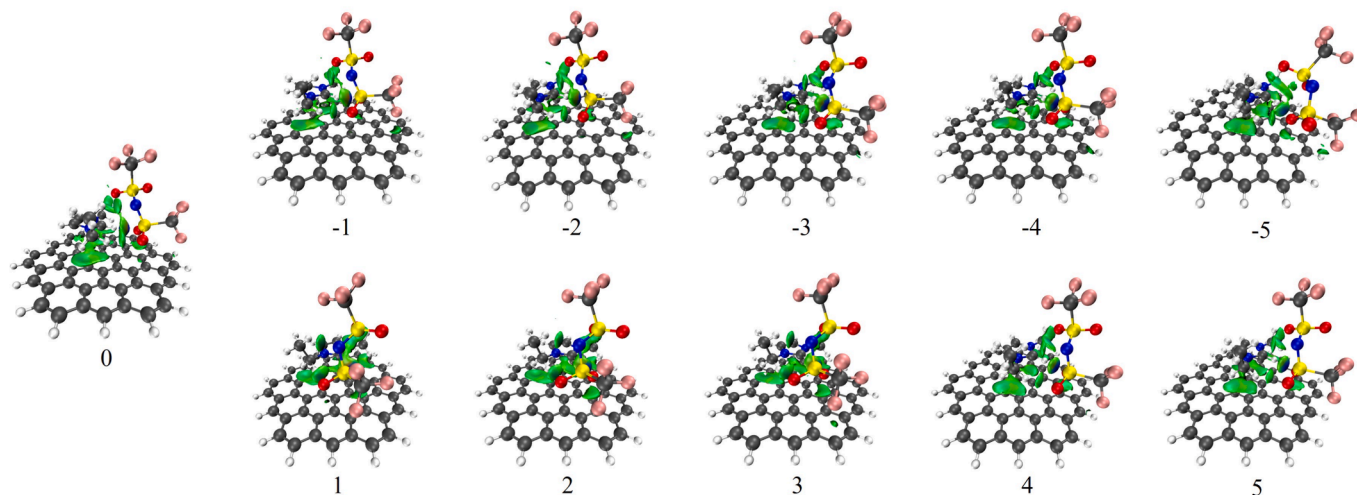


Fig. 3. Diagram of the weak interaction of the *cis* isomer of graphene-[Emim][NTf₂] system under the EEFs in the *x* direction, where the strength of the EEFs is in units of 10⁻³ a.u.

Fig. 4 depicts the nuanced interactions of the *cis* isomer of graphene-[Emim][NTf₂] under the influence of EEFs in the *z* direction. Upon applying the EEFs in this direction, a notable shift in the relative positions of the anions and cations is observed. Specifically, the [NTf₂]⁻ ion tends to migrate away from the graphene in the positive *z* direction, resulting in a diminished weak interaction with the graphene. Conversely, when EEFs are introduced in the negative *z* direction, the [Emim][NTf₂] experiences a force in this direction. This leads to an enhanced weak interaction between the S=O and C-F bonds of [NTf₂]⁻ with the graphene surface. However, with a further increase in the strength of the EEF, the [Emim]⁺ ion exhibits a deflection. The end of its ring, opposite the ethyl chain, shifts away from the graphene surface, leading to a reduction in its weak interaction with the graphene.

The behavior of the *trans* isomer mirrors that of its *cis* counterpart. This similarity is depicted in the weak interaction diagram presented in Fig. 5, which showcases the interactions of the *trans* isomer of graphene-[Emim][NTf₂] under EEFs in the *x* direction. With the introduction of EEFs, the [Emim][NTf₂] is driven towards the graphene surface. Notably, a stable structure becomes untenable once the EEF strength surpasses a specific threshold.

Fig. 6 delineates the weak interactions between the *trans* isomer of graphene-[Emim][NTf₂] and the EEF oriented in the *z* direction. Contrary to the *cis* isomer, the S=O bond at the region of [NTf₂]⁻ ions closer

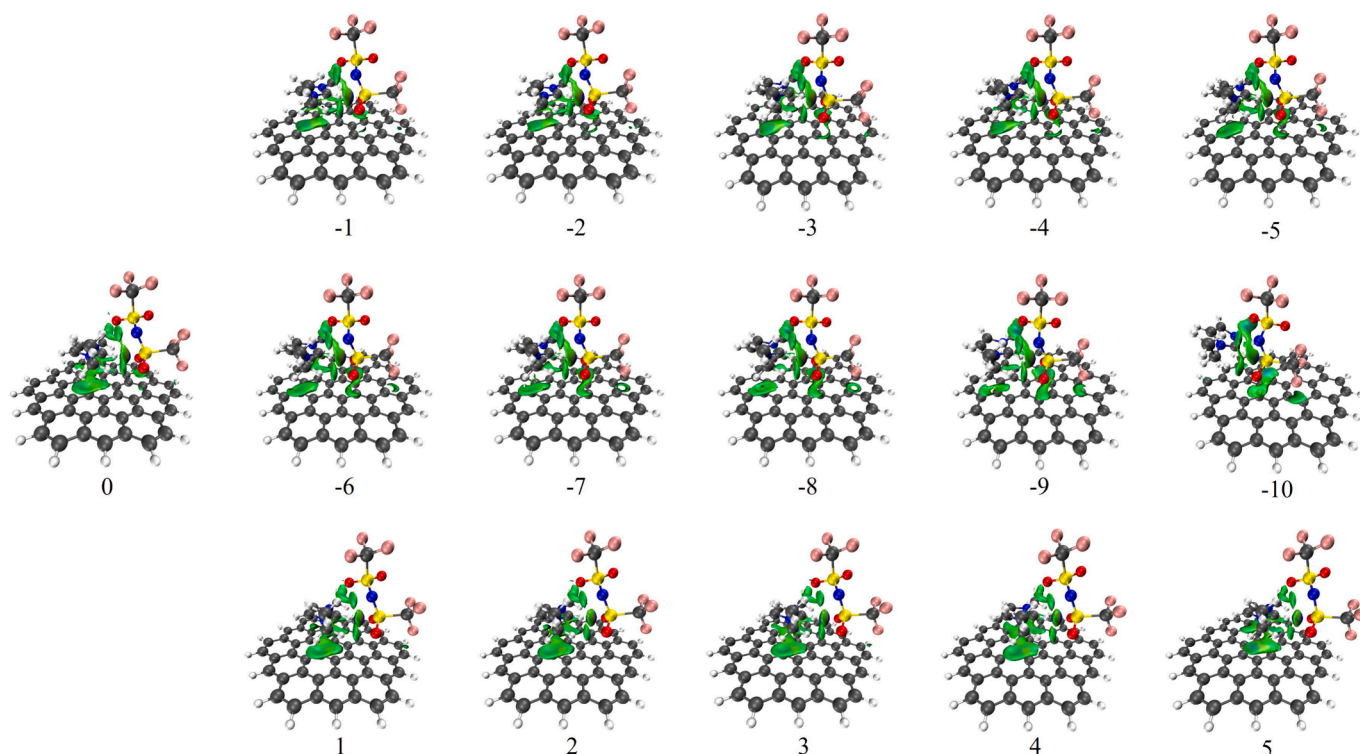


Fig. 4. Diagram of the weak interaction of the *cis* isomer of graphene-[Emim][NTf₂] system under EEFs in the *z* direction, where the strength of the EEFs is in units of 10⁻³ a.u.

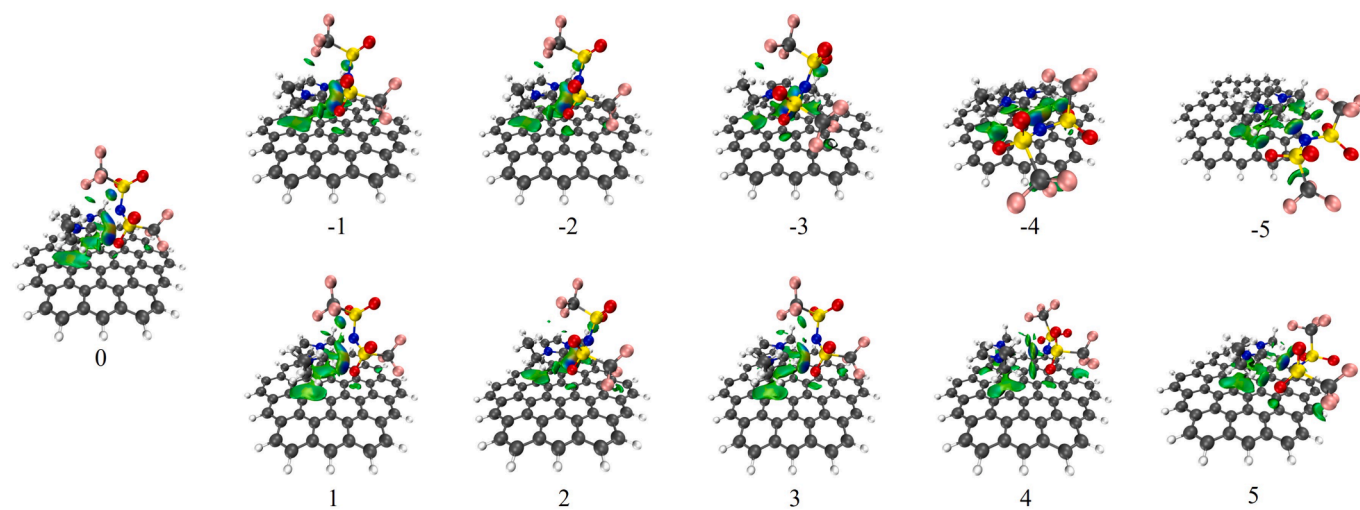


Fig. 5. Diagram of the weak interaction of the *trans* isomer of graphene-[Emim][NTf₂] under EEFs in the *x* direction, where the strength of the EEFs is in units of 10⁻³ a.u.

to the graphene surface does not align with the graphene surface, resulting in a diminished interaction. Upon the application of EEFs in the positive *z* direction, [NTf₂]⁻ readily detaches from the graphene surface. As the EEF strength escalates, [NTf₂]⁻ migrates in the positive *z* direction, further weakening its interaction with the graphene and eventually positioning itself above [Emim]⁺. During this phase, the primary weak interactions within the system involve the N-S and S=O bonds of [NTf₂]⁻ with the methyl groups. When EEFs are applied in the negative *z* direction, the interaction between the S=O and C-F bonds at the region of [NTf₂]⁻ ions closer to the graphene surface and the graphene surface intensifies. A subsequent increase in EEF strength results in a deflection of [Emim]⁺ and a decrease in its interaction with the graphene, while

[NTf₂]⁻ moves closer to the graphene surface, enhancing its attraction. Further amplification of the field strength affects the S=O bond at the region of [NTf₂]⁻ ions further to the graphene surface, fostering a new weak interaction with the graphene. The [Emim]⁺ ion shifts, and the region of [NTf₂]⁻ ions further to the graphene surface approaches the graphene surface. In systems with the *trans* isomer subjected to the EEFs in the positive *z* direction, [NTf₂]⁻ is more susceptible to displacement compared to its *cis* counterpart. This discrepancy is attributed to the inherent stability of the *cis* isomer of [NTf₂]⁻, which exhibits a more robust binding to the graphene surface in the absence of EEFs and is consequently less influenced by them.

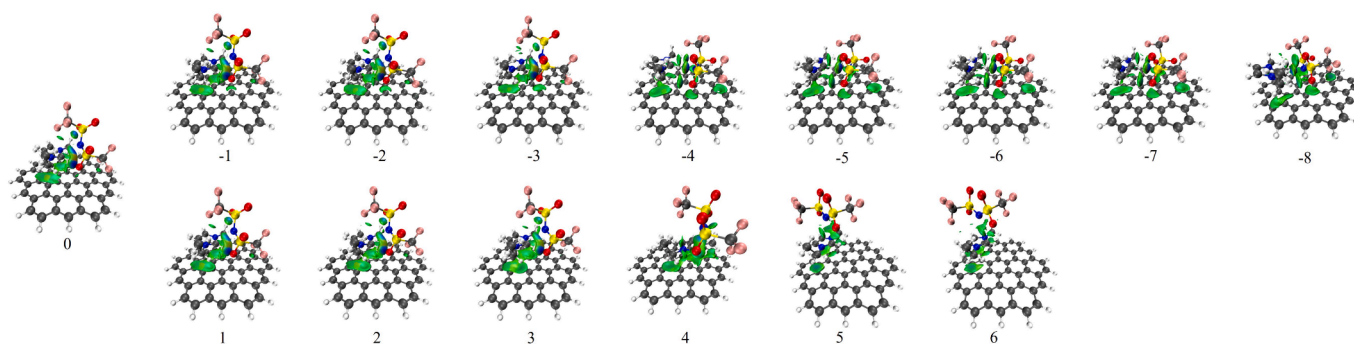


Fig. 6. Diagram of the weak interaction of the *trans* isomer of graphene-[Emim][NTf₂] under EEFs in the *z* direction, where the strength of the EEFs is in units of 10^{-3} a.u.

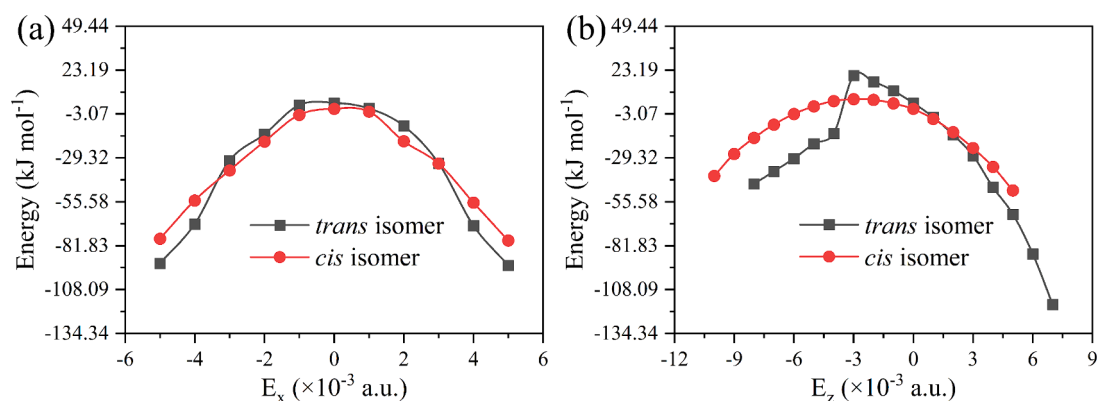


Fig. 7. Changes in energy with EEFs for the graphene-[Emim][NTf₂] with *cis* and *trans* isomer. EEF is in the positive (a) *x* and (b) *z* direction.

3.2. Energy change

Fig. 7 presents the energy variations of the graphene-[Emim][NTf₂] system for both *cis* and *trans* isomers in the absence of EEFs, which are initially 0 kJ mol^{-1} and 3.57 kJ mol^{-1} , respectively. Upon the introduction of EEFs in the positive *x* direction, the energy of the system is perturbed, causing it to decrease as the strength of the EEFs increases. In contrast, when EEFs are applied in the positive *z* direction, the energies for both isomers peak at 5.72 kJ mol^{-1} and $19.90 \text{ kJ mol}^{-1}$ at an EEF strength of -0.003 a.u. , before commencing a downward trend.

In the absence of EEFs, the energy decomposition of the graphene-[Emim][NTf₂] system for both isomers is ascertained using Psi 4 software [56], leveraging the symmetry-adapted perturbation theory-DFT (SAPT(DFT)) at the aug-cc-pvdz level. Table 1 presents a detailed

breakdown of energy interactions involving graphene, [Emim][NTf₂], cation, and anion, where g-[Emim][NTf₂] represents the energy of an interaction of the ion pair with graphene, and [Emim][NTf₂](g) represents the interaction energy between the ions at the graphene surface. Notably, the interaction energies for *cis* and *trans* configurations exhibit disparities. Specifically, the interaction energy between the anion and cation of the *trans* isomer on the graphene surface diminishes from $-339.92 \text{ kJ mol}^{-1}$ to $-334.32 \text{ kJ mol}^{-1}$, while the *cis* configuration remains relatively invariant. The energy components of the graphene-[Emim][NTf₂] complex are predominantly governed by dispersion and exchange, with the dispersion energy between the cation and graphene being the most significant. For both *cis* and *trans* isomers, the interactions between graphene and the anion are primarily governed by induction (accounting for 38.19 % and 34.84 %) and dispersion

Table 1

The interaction energy (in kJ mol^{-1}) of graphene-[Emim][NTf₂] with *cis* and *trans* isomer.

Molecular system	Electrostatics	Exchange	Induction	Delta HF, r (2)	Dispersion	Total SAPT(DFT)
A. Graphene-[Emim][NTf ₂] with <i>cis</i> isomer						
[Emim][NTf ₂]	-348.29	101.25	-39.78	-11.44	-53.76	-340.57
g-[Emim][NTf ₂] ^a	-43.49	107.43	-22.59	-8.52	-115.91	-74.57
[Emim][NTf ₂](g) ^b	-339.90	90.31	-46.98	-15.20	-43.77	-340.34
g-[Emim] ⁺	-57.17	68.52	-40.61	-8.96	-77.75	-107.02
g-[NTf ₂] ⁻	14.58	31.35	-24.96	-1.96	-38.42	-17.44
B. Graphene-[Emim][NTf ₂] with <i>trans</i> isomer						
[Emim][NTf ₂]	-346.32	101.73	-40.51	-11.69	-54.83	-339.92
g-[Emim][NTf ₂]	-41.15	98.51	-19.11	-8.00	-111.11	-72.85
[Emim][NTf ₂](g)	-338.78	97.52	-44.69	-14.52	-48.38	-334.32
g-[Emim] ⁺	-56.97	70.44	-42.51	-9.65	-77.92	-106.97
g-[NTf ₂] ⁻	16.97	21.05	-18.67	-1.44	-33.47	-14.11

^a The energy of an interaction of the ion pair with graphene.

^b The interaction energy between the ions at the graphene surface.

(accounting for 58.80 % and 62.47 %, respectively) [57]. These interactions result in the anion of the *cis* isomer being closer to the graphene surface compared to the *trans* isomer. Moreover, the exchange energy for the *cis* configuration exceeds that of the *trans* by 8.92 kJ·mol⁻¹, underscoring the distinct weak interactions of the S=O bond with the graphene surface, particularly at the region of [NTf₂]⁻ ions closer to the graphene surface.

3.3. Polarization properties

The impact of EEFs on the dipole moment mirrors the trends observed in energy variations. Upon the application of EEFs in the positive *x* direction, the [Emim][NTf₂] shifts on the graphene surface, deviating from its central position. This displacement correlates with an increase in the dipole moment as the strength of the EEFs intensifies. Similarly, when EEFs are applied in the positive *z* direction, the anions migrate accordingly, leading to an elevation in the dipole moment. Conversely, the introduction of EEFs in the negative *z* direction initially reduces the dipole moment, reaching a minimum at -0.003 a.u., before subsequently increasing as depicted in Fig. 8. These trends are congruent with the previously discussed weak interactions, wherein additional EEFs induce structural alterations in the [Emim][NTf₂] structure, thereby influencing the dipole moment.

The behavior of polarizability in response to EEFs closely resembles that of the dipole moment, as illustrated in Fig. 9. Specifically, upon the application of an EEF in the positive *z* direction, the dipole moment reaches its nadir at -0.003 a.u., before subsequently increasing with escalating EEF strength. This phenomenon can be attributed to the system achieving a state of stability at -0.003 a.u. in the presence of EEFs. However, the application of stronger EEFs disrupts this equilibrium, resulting in elevated levels of both dipole moment and polarizability.

The MPI serves as a metric for assessing the modulation of system polarity in the presence of EEFs. As Fig. 10 illustrates, MPI values escalate with increasing EEF strength. This trend is indicative of the charge distribution of the system, which is inherently linked to molecular polarity. Specifically, a more uneven charge distribution engenders either a highly positive or highly negative.

3.4. Vibration spectrum

The VS for graphene-[Emim][NTf₂] system, encompassing both *cis* and *trans* isomers, were computed utilizing the B3LYP/TZVP level of theory in Gaussian 16. Detailed assignments for these spectra are presented in Table 2. In the case of graphene-[Emim][NTf₂] system featuring a *cis* isomer, EEFs oriented positively along the *z* directions induce notable shifts in the VS, as depicted in Fig. 11. Specifically, with

EEFs directed positively along *z* direction, synchronous stretching vibrational peaks of the S=O bond transition from 1051.98 cm⁻¹ and 1074.99 cm⁻¹ (at 0 a.u.) to 1064.92 cm⁻¹ and 1081.91 cm⁻¹ (at 0.005 a. u.), marking blue shifts of 12.94 cm⁻¹ and 6.92 cm⁻¹, respectively. This shift can be attributed to the response of the [NTf₂]⁻ anion to the EEFs, moving in the positive *z* direction. Concurrently, the interaction between the S=O bond in the region of [NTf₂]⁻ ions closer to the graphene surface and the graphene surface diminishes, while the upper S=O bond retains its negligible interaction with the graphene. As EEF intensity.

When EEFs are oriented along the positive *z* direction, the asynchronous stretching vibrational peaks associated with the S=O bond transition from 1250.02 cm⁻¹ and 1267.17 cm⁻¹ (at 0 a.u.) to 1259.43 cm⁻¹ and 1269.69 cm⁻¹ (at 0.005 a.u.), reflecting blue shifts of 9.41 cm⁻¹ and 6.92 cm⁻¹, respectively. This behavior is attributed to the influence of EEFs on the [NTf₂]⁻ anion, which undergoes a shift in the positive *z* direction. Consequently, the weak interaction between the S=O bond in the region of [NTf₂]⁻ ions closer to the graphene surface and the graphene surface diminishes, mirroring the interaction observed in the upper region. This results in a reduced interval between the two vibrational peaks. In contrast, when EEFs are applied in the negative *z* direction, the peaks shift to 1210.59 cm⁻¹ and 1274.28 cm⁻¹ at -0.01 a. u., corresponding to a red shift of 39.43 cm⁻¹ and a blue shift of 7.11 cm⁻¹. The response of the [NTf₂]⁻ anion to the negatively oriented EEFs leads to an enhanced weak interaction with both [Emim]⁺ and the graphene surface. Notably, while both S=O bonds in the region of [NTf₂]⁻ ions closer to the graphene surface exhibit increased weak interactions with the graphene surface under the influence of EEFs, the bonds in the region of [NTf₂]⁻ ions further to the graphene surface display differential behavior. Specifically, one S=O bond interacts weakly with [Emim]⁺, whereas the other remains unaffected by other fragments. This differential behavior results in an expanded interval between the two vibrational peaks.

Upon the application of EEFs oriented along the positive *z* direction, the stretching vibrational peak of the N-S bond transitions from 976.13 cm⁻¹ (at 0 a.u.) to 979.02 cm⁻¹ (at 0.005 a.u.), exhibiting a blue shift of 2.89 cm⁻¹. This shift can be attributed to the response of the [NTf₂]⁻ anion to the EEFs, which results in its movement in the positive *z* direction. Consequently, the weak interaction between the N-S bond and [Emim]⁺ diminishes, leading to the observed blue shift. In contrast, when EEFs are oriented along the negative *z* direction, the vibrational peak relocates to 967.93 cm⁻¹ at -0.01 a.u., undergoing a red shift of 8.20 cm⁻¹. Under these conditions, the interaction of the [NTf₂]⁻ anion with both [Emim]⁺ and the graphene surface intensifies, predominantly due to hydrogen bonding, culminating in the red-shifted vibrational peak.

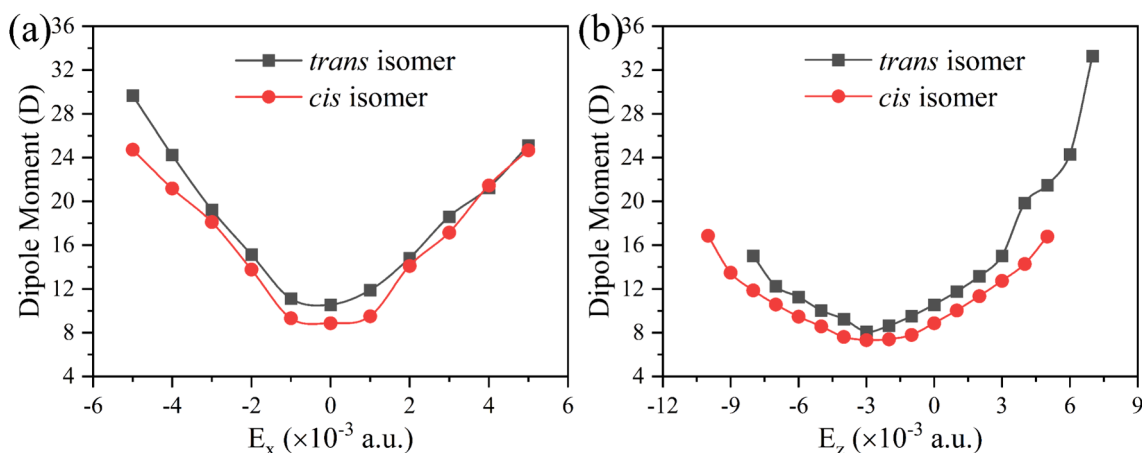


Fig. 8. Changes of dipole moment with EEFs for graphene-[Emim][NTf₂] with *cis* and *trans* isomer. EEF is in the positive (a) *x* and (b) *z* direction.

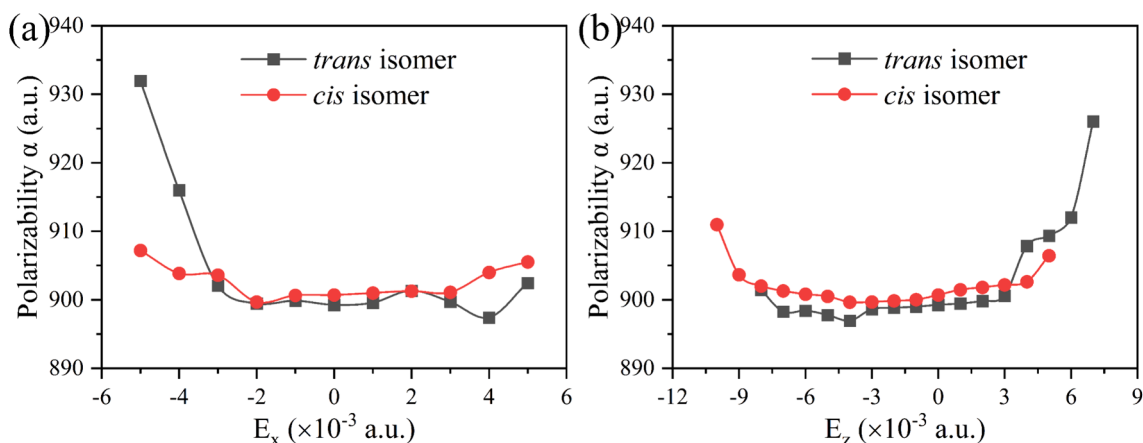


Fig. 9. Changes of polarizability with EEFs for graphene-[Emim][NTf₂] system with *cis* and *trans* isomer. EEF is in the positive (a) *x* and (b) *z* direction.

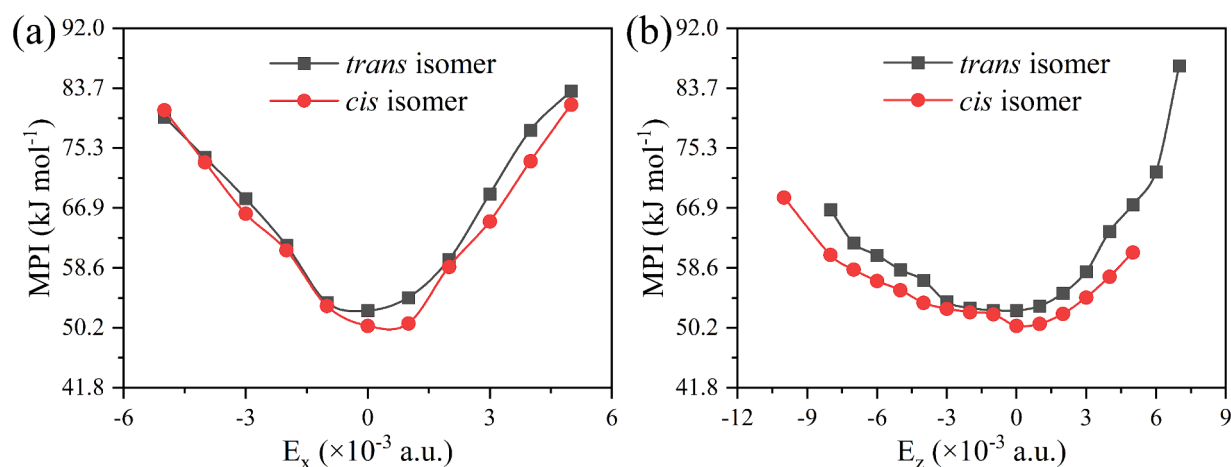


Fig. 10. Changes of MPI with EEFs for graphene-[Emim][NTf₂] system with *cis* and *trans* isomer. EEF is in the positive (a) *x* and (b) *z* direction. electrostatic potential on the molecular surface, thereby amplifying the MPI. The application of EEFs exacerbates this uneven charge distribution, consequently elevating the MPI in proportion to EEF strength.

Table 2

The assignment of VS of graphene-[Emim][NTf₂] system with *cis* and *trans* isomer.

Cis Structure		Trans Structure		Assignment
Frequency $\nu(\text{cm}^{-1})$	Intensity	Frequency $\nu(\text{cm}^{-1})$	Intensity	
903.76	166.3332	904.77	168.7423	graphene $\omega(\text{Cg-Hg})$
976.13	276.0080	972.44	343.5523	N-S str
1051.98	127.0900	1064.16	85.0720	S=O synchronous str
1074.99	402.7876	1080.64	154.3206	S=O synchronous str
1160.01	145.6151	1167.89	123.6462	S-C & C-F str
1177.66	68.4043	1173.26	121.3161	C-F str
1182.47	210.4030	1193.52	157.6756	C-F str
1184.28	158.2887	1190.69	53.8140	S-C & C-F str
1210.12	169.4513	1205.32	394.8959	C-F str
1250.02	153.8208	1268.46	104.7278	S=O asynchronous str
1267.17	310.9794	1301.99	441.2779	S=O asynchronous str
3203.91	109.1372	3282.83	50.4860	C2-H str

Similarly, for the C2-H bond, the stretching vibrational peak moves from 3203.91 cm^{-1} (at 0 a.u.) to 3218.43 cm^{-1} (at 0.005 a.u.) under the EEFs in positive *z* direction, reflecting a blue shift of 14.52 cm^{-1} . This shift arises from the diminished interaction between [Emim]⁺ and [NTf₂]⁻ in the presence of EEFs. However, with EEFs oriented in the negative *z* direction, the peak first red-shifts slightly to 3203.59 cm^{-1} at

-0.003 a.u., and subsequently blue-shifts significantly to 3232.19 cm^{-1} at -0.01 a.u. This behavior is indicative of the augmented weak interaction between [NTf₂]⁻ and [Emim]⁺, where hydrogen bonding plays a pivotal role, leading to the observed vibrational shifts.

When EEFs are applied along the positive *z* direction, the stretching vibrational peaks for the C-S and C-F bonds exhibit a shift. Specifically, the frequency range transitions from an interval of 1160.01 cm^{-1} to 1210.12 cm^{-1} (at 0 a.u.) to an interval of 1153.87.

For the graphene-[Emim][NTf₂] system with a *trans* isomer configuration, as depicted in Fig. 12, the VS behavior mirrors that of its *cis* counterpart. Specifically, under the influence of EEFs oriented in the positive *z* direction, the synchronous stretching vibrational peaks of the S=O bond transition from 1064.16 cm^{-1} and 1080.64 cm^{-1} (at 0 a.u.) to 1077.01 cm^{-1} and 1082.59 cm^{-1} (at 0.007 a.u.). This corresponds to blue shifts of 12.85 cm^{-1} and 1.95 cm^{-1} , respectively. Such shifts are attributed to the positional adjustments of the [NTf₂]⁻ ion in response to the EEFs, leading to a blue shift in the vibrational peaks. Notably, the weak interaction between the S=O bond of the region of [NTf₂]⁻ ions closer to the graphene surface and the graphene surface diminishes, especially at 0.005 a.u. As the strength of the EEFs increases, these weak interactions with the graphene surface converge, narrowing the gap between the two synchronous stretching vibrational peaks. Conversely, when EEFs are applied in the negative *z* direction, the peaks shift to 1057.95 cm^{-1} and 1065.34 cm^{-1} at -0.008 a.u., marking red shifts of 6.21 cm^{-1} and 15.30 cm^{-1} . In this scenario, the movement of the

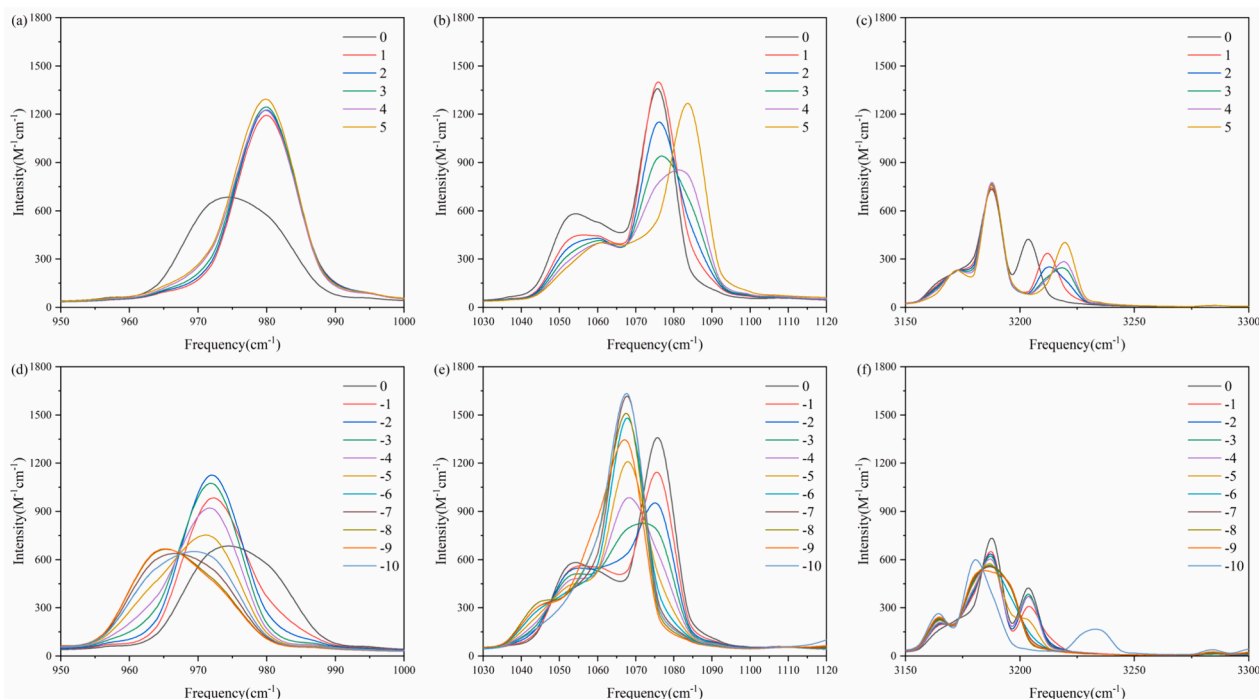


Fig. 11. The VS of graphene-[Emim][NTf₂] system with *cis* isomer. The interval of frequency is (a) 950 cm⁻¹ to 1000 cm⁻¹, (b) 1030 cm⁻¹ to 1120 cm⁻¹, and (c) 3100 cm⁻¹ to 3250 cm⁻¹ under EEFs in the positive *z* direction, and (d) 950 cm⁻¹ to 1000 cm⁻¹, (e) 1030 cm⁻¹ to 1120 cm⁻¹, and (f) 3100 cm⁻¹ to 3250 cm⁻¹ under EEFs in the negative *z* direction. The strength of the EEFs is in units of 10⁻³ a.u., rises, the interactions between both S=O bonds and the graphene surface converge, narrowing the gap between their vibrational peaks. Conversely, when EEFs are applied in the negative *z* direction, the peaks shift to 1048.88 cm⁻¹ and 1067.17 cm⁻¹ at -0.01 a.u., reflecting red shifts of 3.10 cm⁻¹ and 7.82 cm⁻¹. This behavior is due to the movement of the [NTf₂]⁻ anion in the negative *z* direction under the influence of EEFs, leading to a red shift in the vibrational peaks of the two S=O bonds. (For interpretation of the references to colour in this figure legend, the reader is referred to the web version of this article.)

[NTf₂]⁻ ion in the negative *z* direction induces a red shift in the vibrational peaks. It's noteworthy that only one of the S=O bonds in the region of [NTf₂]⁻ ions closer to the graphene surface exhibits weak interaction with the graphene surface, while the other engages weakly with the [Emim]⁺ ion, leading to an increased interval between the vibrational peaks.

When subjected to EEFs oriented in the positive *z* direction, the asynchronous stretching vibrational peaks of the S=O bond transition from 1268.46 cm⁻¹ and 1301.99 cm⁻¹ to 1268.50 cm⁻¹ and 1293.55 cm⁻¹ at 0.007 a.u. This results in a red shift of 8.44 cm⁻¹ for one peak, while the other remains largely invariant. Such shifts can be attributed to the positional adjustments of the [NTf₂]⁻ ion in response to the EEFs. Specifically, the S=O bond in the region of [NTf₂]⁻ ions closer to the graphene surface exhibits an enhanced weak interaction with [Emim]⁺, compounded by its existing weak interaction with the ethyl chain, leading to a pronounced red shift. Conversely, under EEFs oriented in the negative *z* direction, the vibrational peaks shift to 1265.27 cm⁻¹ and 1308.39 cm⁻¹ at -0.003 a.u., followed by 1267.84 cm⁻¹ and 1280.70 cm⁻¹ at -0.008 a.u. This behavior contrasts with the *cis* configuration, as the *trans* isomeric [NTf₂]⁻ ion interacts concurrently with the cationic ethyl chain, resulting in a subtly distinct structure. As the [NTf₂]⁻ ion adjusts to the EEFs in the negative *z* direction, its weak interactions with both [Emim]⁺ and the graphene surface intensify. For EEF strengths below 0.003 a.u., the upper S=O bond in the [NTf₂]⁻ ion primarily engages weakly with the cationic methyl group, mirroring the vibrational peak behaviors of the *cis* configuration. However, at EEF strengths exceeding 0.003 a.u., this bond undergoes significant displacement in the negative *z* direction. It not only retains its weak interaction with the cationic methyl group but also amplifies its weak interaction with the graphene surface. Concurrently, the interaction between the alternate S=O bond pair and [Emim]⁺ diminishes, leading to a blue shift in the

vibrational peaks.

Upon the application of EEFs oriented along the positive *z* direction, the stretching vibrational peak of the N-S bond transitions from 972.44 cm⁻¹ to 974.04 cm⁻¹ at 0.007 a.u., marking a blue shift of 1.60 cm⁻¹. This shift is attributed to a significant reduction in the interaction between the N-S bond and [Emim]⁺, transitioning from a hydrogen bond (represented in blue) to a weaker interaction (represented in green). Conversely, under EEFs oriented along the negative *z* direction, the vibrational peak first shifts to 968.43 cm⁻¹ at -0.003 a.u. (a red shift of 4.01 cm⁻¹) and subsequently to 979.68 cm⁻¹ at -0.008 a.u. (a blue shift of 7.24 cm⁻¹). This behavior is influenced by the movement of the [NTf₂]⁻ ion in the negative *z* direction, intensifying its interaction with both [Emim]⁺ and the graphene surface. For EEF strengths below 0.003 a.u., the N-S bond predominantly forms hydrogen bonds with [Emim]⁺, inducing the observed red shift. However, at strengths exceeding 0.003 a.u., the N-S bond approaches the graphene surface, leading to a weak interaction and a consequent blue shift in its vibrational peak.

For the C2-H bond, under EEFs oriented along the positive *z* direction, its vibrational peak shifts from 3282.83 cm⁻¹ to 3299.31 cm⁻¹ at 0.007 a.u., marking a blue shift of 16.48 cm⁻¹. In contrast, under the influence of EEFs in the negative *z* direction, the peak first transitions to 3284.06 cm⁻¹ at -0.003 a.u. (a blue shift of 1.23 cm⁻¹) and then dramatically to 3161.05 cm⁻¹ at -0.008 a.u. (a red shift of 121.78 cm⁻¹). This pronounced red shift at -0.008 a.u. is primarily due to the augmented interaction between the C2-H bond, [NTf₂]⁻, and graphene. At EEF strengths below 0.003 a.u., the interaction between [NTf₂]⁻ and [Emim]⁺ intensifies, predominantly due to hydrogen bonding, resulting in a blue shift for the C2-H bond. However, at higher EEF strengths, the significant displacement of the N-S bond towards the graphene surface diminishes the interaction between the C2-H bond and [NTf₂]⁻, causing the observed red shift.

When EEFs are applied along the positive *z* direction, the frequency

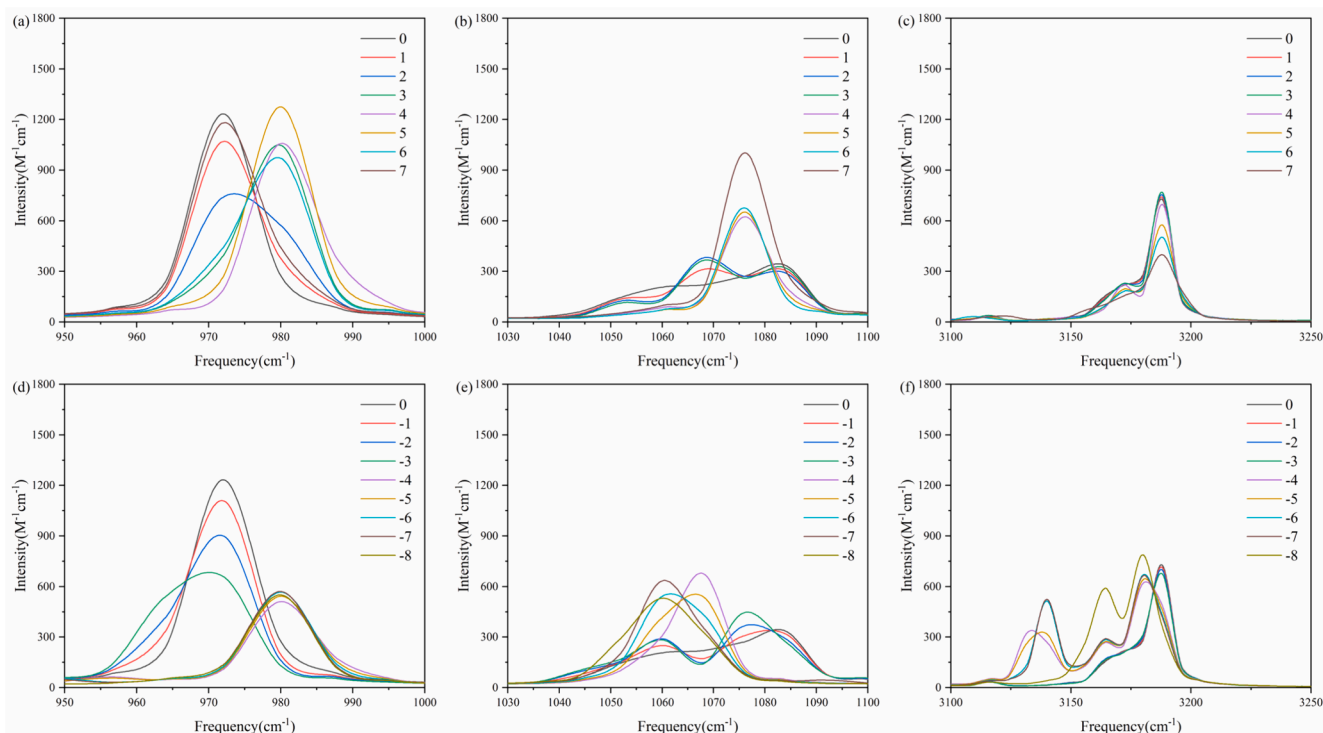


Fig. 12. The VS of graphene-[Emim][NTf₂] with *trans* isomer. The interval of frequency is (a) 950 cm⁻¹ to 1000 cm⁻¹, (b) 1030 cm⁻¹ to 1100 cm⁻¹, and (c) 3100 cm⁻¹ to 3250 cm⁻¹ under EEFs in the positive *z* direction, and (d) 950 cm⁻¹ to 1000 cm⁻¹, (e) 1030 cm⁻¹ to 1120 cm⁻¹, and (f) 3100 cm⁻¹ to 3250 cm⁻¹ under EEFs in the negative *z* direction. The strength of the EEFs is in units of 10⁻³ a.u.cm⁻¹ to 1191.41 cm⁻¹ (at 0.005 a.u.), manifesting an overall red shift. Conversely, under the influence of EEFs oriented along the negative *z* direction, the stretching vibrational frequencies for the C-S and C-F bonds shift to 1153.80 cm⁻¹ and 1217.30 cm⁻¹ at -0.003 a.u., and further to 1133.16 cm⁻¹ and 1162.05 cm⁻¹ at -0.01 a.u. This behavior also indicates a general trend of red shifting for the vibrational intervals. (For interpretation of the references to colour in this figure legend, the reader is referred to the web version of this article.)

interval for the stretching vibrations of the C-S and C-F bonds shifts from 1167.89 cm⁻¹ to 1205.32 cm⁻¹ to a narrower range of 1159.72 cm⁻¹ to 1182.60 cm⁻¹ at 0.007 a.u., indicating an overall red shift. Conversely, under the influence of EEFs along the negative *z* direction, the frequency for the C-S bond shifts to 1133.16 cm⁻¹ and 1144.70 cm⁻¹ at -0.003 a.u. and -0.008 a.u., respectively, while the C-F bond shifts to 1218.68 cm⁻¹ and 1237.76 cm⁻¹. This results in a red shift for the lower boundary and a blue shift for the upper boundary of the frequency interval, thereby widening the interval. The observed changes in the C-F bond can be attributed to the increased influence of the cationic carbon chain and graphene.

For the graphene-[Emim][NTf₂] system, the exchange energy associated with the *cis* isomer is 107.43 kJ•mol⁻¹, whereas the *trans* isomer exhibits an exchange energy of 98.51 kJ•mol⁻¹. This difference in exchange energy influences the behavior of graphene-[Emim][NTf₂] under EEFs directed along the negative *z* direction. The primary distinction in the VS shifts between the *cis* and *trans* structures can be attributed to the specific isomer of [NTf₂]⁻ interacting with graphene. In the *trans* configuration, the S=O bond is positioned further from the graphene surface compared to its *cis* counterpart. Consequently, when EEFs directed along the negative *z* direction are applied, the *trans* isomer of [NTf₂]⁻ undergoes a more pronounced deformation from its upright orientation. This results in the S=O and C-F bonds, located at the region of [NTf₂]⁻ ions further to the graphene surface, experiencing weak interactions with the graphene surface. Such interactions induce alterations in the VS, manifesting as a trend shift at -0.003 a.u. In contrast, the *cis* isomer of [NTf₂]⁻ remains relatively stable under similar conditions, leading to a more consistent VS response upon EEF application.

4. Conclusions

This work employs DFT calculations to investigate the influence of EEFs on the polarization properties and VS of the *cis* and *trans* isomers of [Emim][NTf₂] on a graphene surface. The DFT calculations reveal that both the dipole moment and polarizability of the graphene-[Emim][NTf₂] system in its *cis* and *trans* configurations are subject to modulation by EEFs. Specifically, these properties increase under EEFs applied in the *x* direction and the positive *z* direction. Conversely, under EEFs in the negative *z* direction, an initial decrease followed by an increase in these properties is observed. To elucidate the property of inter-ion interactions under EEFs, such as hydrogen bonding and van der Waals forces, the IGM was utilized to detail the variation of these interactions in response to the direction and intensity of the EEFs. The VS of [Emim][NTf₂] on the graphene surface, spanning the range of 10–3500 cm⁻¹, was meticulously calculated to systematically investigate the impact of EEFs on the VS of the graphene-[Emim][NTf₂] system. The regulation of the VS by EEFs in both *cis* and *trans* isomers is primarily achieved through alterations in the interactions between molecular fragments within the system. In the *cis* isomer under an EEF in positive *z* direction, the synchronous and alternating stretching vibrational peaks of the S=O bond, the N-S bond, and the C2-H bond all exhibit a blue shift. This shift is mainly due to the reduced interaction between these functional groups and their adjacent fragments. In contrast, under an EEF in negative *z* direction, these vibrational peaks undergo a red shift, primarily because of increased interactions of these functional groups on the anion [NTf₂]⁻ with other fragments. The stretching vibrational peaks of the C2-H bond on the cation [Emim]⁺ initially red shift and then blue shift. This phenomenon is triggered by the displacement of the imidazole ring of [Emim]⁺ when the EEF strength exceeds 0.003 a.u. In the *trans* isomer, similar trends are observed under an EEF in positive *z*

direction. However, the alternating stretching vibrational peaks of the S=O bond display both blue and red shifts, reflecting the unique anion structure of the *trans* configuration. A comparative analysis of the vibrational peaks caused by the same functional groups in the *cis* and *trans* isomers, combined with an examination of the interaction energy of the system, reveals that the exchange energy between graphene and the [Emim][NTf₂] ion pair in the *cis* isomer is 107.43 kJ•mol⁻¹, while in the *trans* isomer, it is 98.51 kJ•mol⁻¹, lower by 8.92 kJ•mol⁻¹. This discrepancy leads to distinct regulatory effects in the *cis* and *trans* isomers. This work provides a comprehensive study of the polarization properties and VS of the *cis* and *trans* isomers of the graphene-[Emim][NTf₂] system under EEFs, the findings underscore the importance of considering the effects of EEFs in the design and application of graphene-ILs system in the field of energy harvesting.

CRedit authorship contribution statement

Yongji Guan: Writing – review & editing, Writing – original draft, Visualization, Software, Methodology, Investigation, Funding acquisition, Formal analysis, Data curation, Conceptualization. **Chuyu Li:** Visualization, Software, Methodology, Investigation. **Xin Han:** Software, Methodology, Data curation. **Huanwang Jing:** Software. **Fulong Yang:** Funding acquisition. **Xiaoping Zhang:** Supervision, Project administration, Funding acquisition, Conceptualization. **Youquan Deng:** Supervision, Project administration, Funding acquisition, Conceptualization.

Declaration of competing interest

The authors declare that they have no known competing financial interests or personal relationships that could have appeared to influence the work reported in this paper.

Data availability

Data will be made available on request.

Acknowledgements

The authors acknowledge the financial support of this work from the Fund for Less Developed Regions of the National Natural Science Foundation of China (62061025), Natural Science Foundation of Gansu Province for Young Scientists (23JRRA1112) and the Scientific Research Foundation of Lanzhou University for the Talented Young Scholars (561120207).

References

- [1] J.S. Wilkes, *Green Chem.* 4 (2002) 73.
- [2] C. Austen Angell, Y. Ansari, Z. Zhao, *Faraday Discuss.* 154 (2012) 9.
- [3] T. Welton, *Biophys. Rev.* 10 (2018) 691.
- [4] T. Welton, *Chem. Rev.* 99 (1999) 2071.
- [5] P. Wasserscheid, W. Keim, *Angew. Chem. Int. Ed.* 39 (2000) 3772.
- [6] K.R. Seddon, *Nat. Mater.* 2 (2003) 363.
- [7] J.P. Hallett, T. Welton, *Chem. Rev.* 111 (2011) 3508.
- [8] X. Han, D.W. Armstrong, *Acc. Chem. Res.* 40 (2007) 1079.
- [9] A. Berthod, M.J. Ruiz-Ángel, S. Carda-Broch, *J. Chromatogr. A* 1184 (2008) 6.
- [10] R. Sheldon, *Chem. Commun.* (2001) 2399.
- [11] J. Dupont, R.F. de Souza, P.A.Z. Suarez, *Chem. Rev.* 102 (2002) 3667.
- [12] D. Zhao, M. Wu, Y. Kou, E. Min, *Catal. Today* 74 (2002) 157.
- [13] T. Welton, *Coord. Chem. Rev.* 248 (2004) 2459.
- [14] V.I. Pärvulescu, C. Hardacre, *Chem. Rev.* 107 (2007) 2615.
- [15] H. Olivier-Bourbigou, L. Magna, D. Morvan, *Appl. Catal. A* 373 (2010) 1.
- [16] M.C. Buzzeo, R.G. Evans, R.G. Compton, *ChemPhysChem* 5 (2004) 1106.
- [17] P. Hapiot, C. Lagrost, *Chem. Rev.* 108 (2008) 2238.
- [18] M. Armand, F. Endres, D.R. MacFarlane, H. Ohno, B. Scrosati, *Nat Mater* 8 (2009) 621.

- [19] H. Liu, Y. Liu, J. Li, *Phys. Chem. Chem. Phys.* 12 (2010) 1685.
- [20] W. Kong, L. Cheng, X. He, Z. Xu, X. Ma, Y. He, L. Lu, X. Zhang, Y. Deng, *Microfluid. Nanofluid.* 18 (2014) 1299.
- [21] Q. Shao, J. Jia, Y. Guan, X. He, X. Zhang, *J. Chem. Phys.* 144 (2016) 124703.
- [22] X.D. He, W.B. Qiang, J.B. Wu, Q.F. Shao, P.F. Cao, L. Cheng, X.P. Zhang, Y.Q. Deng, *J. Phys. D Appl. Phys.* 50 (2017) 465002.
- [23] Y. Guan, Q. Shao, W. Chen, J. Zhang, X. Zhang, Y. Deng, *J. Mater. Chem. A* 6 (2018) 11941.
- [24] Y. Guan, W. Chen, J. Zhang, F. Yang, C. Du, X. Zhang, Y. Deng, *J. Phys. Chem. C* 123 (2019) 6981.
- [25] X.D. Hu, S.G. Zhang, Y. Liu, C. Qu, L.J. Lu, X.Y. Ma, X.P. Zhang, Y.Q. Deng, *Appl. Phys. Lett.* 99 (2011).
- [26] Y.J. Guan, Q.F. Shao, W.Q. Chen, S.M. Liu, X.P. Zhang, Y.Q. Deng, *J. Phys. Chem. C* 121 (2017) 23716.
- [27] X. Hu, S. Zhang, C. Qu, Q. Zhang, L. Lu, X. Ma, X. Zhang, Y. Deng, *Soft Matter* 7 (2011) 5941.
- [28] X. He, Q. Shao, P. Cao, W. Kong, J. Sun, X. Zhang, Y. Deng, *Lab Chip* 15 (2015) 1311.
- [29] G. Kaur, H. Kumar, M. Singla, *J. Mol. Liq.* 351 (2022) 118556.
- [30] J. Zhang, Y. Guan, J. Wang, F. Yang, H. Jing, X. Zhang, Y. Deng, *J. Mol. Liq.* 311 (2020) 113340.
- [31] H. Shirota, M. Ando, S. Kakinuma, K. Takahashi, *Bull. Chem. Soc. Jpn.* 93 (2020) 1520.
- [32] V.H. Paschoal, L.F.O. Faria, M.C.C. Ribeiro, *Chem. Rev.* 117 (2017) 7053.
- [33] H. Shirota, S. Kakinuma, K. Takahashi, A. Tago, H. Jeong, T. Fujisawa, *Bull. Chem. Soc. Jpn.* 89 (2016) 1106.
- [34] K. Fumino, S. Reimann, R. Ludwig, *Phys. Chem. Chem. Phys.* 16 (2014) 21903.
- [35] E.W. Castner Jr., J.F. Wishart, H. Shirota, *Acc. Chem. Res.* 40 (2007) 1217.
- [36] N.E. Heimer, R.E. Del Sesto, Z. Meng, J.S. Wilkes, W.R. Carper, *J. Mol. Liq.* 124 (2006) 84.
- [37] R.S. Booth, C.J. Annesley, J.W. Young, K.M. Vogelhuber, J.A. Boatz, J.A. Stearns, *Phys. Chem. Chem. Phys.* 18 (2016) 17037.
- [38] S. Vyas, C. Dreyer, J. Slingsby, D. Bicknase, J.M. Porter, C.M. Maupin, *J. Phys. Chem. A* 118 (2014) 6873.
- [39] C. Roth, S. Chatzipapadopoulos, D. Kerlé, F. Friedriszik, M. Lütgens, S. Lochbrunner, O. Kühn, R. Ludwig, *New J. Phys.* 14 (2012) 105026.
- [40] J. Grondin, J.-C. Lassègues, D. Cavagnat, T. Buffeteau, P. Johansson, R. Holomb, *J. Raman Spectrosc.* 42 (2011) 733.
- [41] K. Fumino, V. Fossog, P. Stange, K. Wittler, W. Polet, R. Hempelmann, R. Ludwig, *ChemPhysChem* 15 (2014) 2604.
- [42] G. Velupula, R. Phillipson, J.X. Lian, D. Cornil, P. Walke, K. Verguts, S. Brems, I. H. Uji, S. De Gendt, D. Beljonne, R. Lazzaroni, K.S. Mali, S. De Feyter, *ACS Nano* 13 (2019) 3512.
- [43] Y. Guan, J. Zhang, J. Wang, F. Yang, H. Jing, X. Zhang, Y. Deng, *J. Mol. Liq.* 311 (2020) 113353.
- [44] C. Bardak, A. Atac, F. Bardak, *J. Mol. Liq.* 273 (2019) 314.
- [45] Y. Guan, R. Clark, F. Philippi, X. Zhang, T. Welton, *J. Chem. Phys.* 156 (2022) 204312.
- [46] R. Clark, M.V. Domaros, A.J.S. McIntosh, A. Luzar, B. Kirchner, T. Welton, *J. Chem. Phys.* 151 (2019) 164503.
- [47] F.J. Carmona Esteve, Y. Zhang, Y.J. Colón, E.J. Maginn, *J. Phys. Chem. B* 127 (2023) 4623.
- [48] T. Lu, Molclus program, Version 1.9, <http://www.keinsci.com/research/molclus.html>.
- [49] M.J. Frisch, G.W. Trucks, H.B. Schlegel, G.E. Scuseria, M.A. Robb, J.R. Cheeseman, G. Scalmani, V. Barone, G.A. Petersson, H. Nakatsuji, X. Li, M. Caricato, A.V. Marenich, J. Bloino, B.G. Janesko, R. Gomperts, B. Mennucci, H.P. Hratchian, J.V. Ortiz, A.F. Izmaylov, J.L. Sonnenberg, Williams, F. Ding, F. Lipparini, F. Egidi, J. Goings, B. Peng, A. Petrone, T. Henderson, D. Ranasinghe, V.G. Zakrzewski, J. Gao, N. Rega, G. Zheng, W. Liang, M. Hada, M. Ehara, K. Toyota, R. Fukuda, J. Hasegawa, M. Ishida, T. Nakajima, Y. Honda, O. Kitao, H. Nakai, T. Vreven, K. Throssell, J.A. Montgomery Jr., J.E. Peralta, F. Ogliaro, M.J. Bearpark, J.J. Heyd, E.N. Brothers, K.N. Kudin, V.N. Staroverov, T.A. Keith, R. Kobayashi, J. Normand, K. Raghavachari, A.P. Rendell, J.C. Burant, S.S. Iyengar, J. Tomasi, M. Cossi, J.M. Millam, M. Klene, C. Adamo, R. Cammi, J.W. Ochterski, R.L. Martin, K. Morokuma, O. Farkas, J.B. Foresman, D.J. Fox, Wallingford, CT, 2016.
- [50] A. Schäfer, C. Huber, R. Ahlrichs, *J. Chem. Phys.* 100 (1994) 5829.
- [51] S. Grimme, J. Antony, S. Ehrlich, H. Krieg, *J. Chem. Phys.* 132 (2010).
- [52] C. Lefebvre, G. Rubez, H. Khartabil, J.-C. Boisson, J. Contreras-García, E. Hénon, *Phys. Chem. Chem. Phys.* 19 (2017) 17928.
- [53] Z. Liu, T. Lu, Q. Chen, *Carbon* 171 (2021) 514.
- [54] T. Lu, F. Chen, *J. Comput. Chem.* 33 (2012) 580.
- [55] W. Humphrey, A. Dalke, K. Schulten, *J. Mol. Graphics* 14 (1996) 33.
- [56] R.M. Parrish, L.A. Burns, D.G.A. Smith, A.C. Simmonett, A.E. DePrince III, E. G. Hohenstein, U. Bozkaya, A.Y. Sokolov, R. Di Remigio, R.M. Richard, J. F. Gonthier, A.M. James, H.R. McAlexander, A. Kumar, M. Saitow, X. Wang, B. P. Pritchard, P. Verma, H.F. Schaefer III, K. Patkowski, R.A. King, E.F. Valeev, F. A. Evangelista, J.M. Turney, T.D. Crawford, C.D. Sherrill, *J. Chem. Theory Comput.* 13 (2017) 3185.
- [57] E.I. Izgorodina, D.R. MacFarlane, *J. Phys. Chem. B* 115 (2011) 14659.